JOURNAL OF GEOPHYSICAL RESEARCH, VOL. 104, NO. D21, PAGES 26,547–26,563, NOVEMBER 20, 1999

Influence of synoptic waves on column ozone during Arctic summer 1997

Matthew H. Hitchman, Marcus L. Buker, and Gregory J. Tripoli

Department of Atmospheric and Oceanic Sciences, University of Wisconsin-Madison

Abstract. The influence of synoptic waves on column ozone over Alaska during the summer of 1997 is explored using observations of ozone and meteorological quantities, a nonhydrostatic three-dimensional model, and theory. From early May to early August, column ozone over Fairbanks declined from 450 to 250 Dobson Units, while 300 hPa heights rose from 8500 to 9500 m. Time series of daily column ozone and 300 hPa heights are correlated at -0.78. Week-to-week variations contribute strongly to this anticorrelation, with column ozone increasing as a trough approaches. Case studies of synoptic scale waves show that they disturb the lower stratosphere, stretching and folding tropospheric and stratospheric air during their life cycles. Mesoscale resolution simulations with the University of Wisconsin Nonhydrostatic Modeling System (UW-NMS) were carried out in support of NASA's Photochemistry of Ozone Loss in the Arctic Region in Summer (POLARIS) campaigns. Layered ozone structures in an ER2 stairstep flight are represented fairly well by the UW-NMS. Two ozone fields were transported in the model, with one subject to a sink below the dynamical tropopause. UW-NMS ozone distributions, a simple box model, and a Stokes drift argument support the idea that synoptic waves cause a poleward and downward flow of ozone through the high latitude tropopause throughout the year. Planetary wave transport of ozone from the tropics is much reduced in the summer. Net transport out of the high latitude stratosphere likely contributes to column ozone decline during summer.

1. Introduction

During the boreal summer of 1997, column ozone over Fairbanks (65°N, 155°W; Figure 1) declined from ~450 Dobson Units (DU) in early May to ~250 DU in Early August (1 DU = 1 milli-atm-cm of ozone). This drop of 200 DU in 3 months (-60 DU month^{-1}) is comparable to the climatological rate of increase of column ozone over Alaska during January and February [*Bojkov*, 1988]. Winter accumulation is associated with breaking planetary Rossby waves, which advect sheets of tropical, ozone-rich air poleward and downward, around the edge of the polar vortex and into the midlatitude surf zone [e.g., *Leovy et al.*, 1985; *Harvey et al.*, 1999]. This planetary wave activity and its associated ozone transport ceases in late spring as mean winds become easterly. Annually persistent westerly winds near the tropopause support synoptic scale waves (~1000-5000 km wavelengths) all year. These waves are evanescent into the lower stratosphere and facilitate a poleward and downward Lagrangian flow [e.g., *Kida*, 1977; *Wallace*, 1978]. Here we explore the possibility that seasonal changes in net ozone transport contribute toward the summer decline of column ozone.

Evidence for a poleward and downward flow in the lower stratosphere, the "Brewer-Dobson circulation", includes the distribution of radioactive debris [*Feely and Spar*, 1960], volcanic aerosol [*Dyer and Hicks*, 1968], water vapor [*Brewer*, 1949], and ozone [*Dobson*, 1956]. Although it is challenging to calculate accurate net radiative heating rates in the summer polar lower stratosphere, evidence suggests that net cooling of ~0.2-0.5 K/d prevails near 500 K [e.g., *Newell et al.*, 1974, Table 6.3; *Kiehl and Solomon*, 1986; *Rosenfield et al.*, 1994; *Eluskiewicz et al.*, 1996; *Mlynczak et al.*, 1999].

Using seasonally and zonally averaged aerosol patterns, *Hitchman et al.* [1994] argued that air is transported rather easily out of the tropics into high latitudes all year in the first scale height above the tropopause, the "lower transport regime". This zonally symmetric poleward-downward flow is the net result of complex air motions involving monsoon structures, extratropical synoptic waves, and a variety of small-scale processes. *Davies et al.* [1998] showed a striking example of air parcels from the upper tropospheric Asian monsoon arriving near the tropopause over Wales. *Postel and Hitchman* [1999] created a climatology of Rossby wave breaking across the subtropical tropopause at 350 K. During northern summer, synoptic waves in the subtropical westerly jet interact with divergent outflow

Paper number 1999JD900471.
0148-0227/99/1999JD900471$09.00

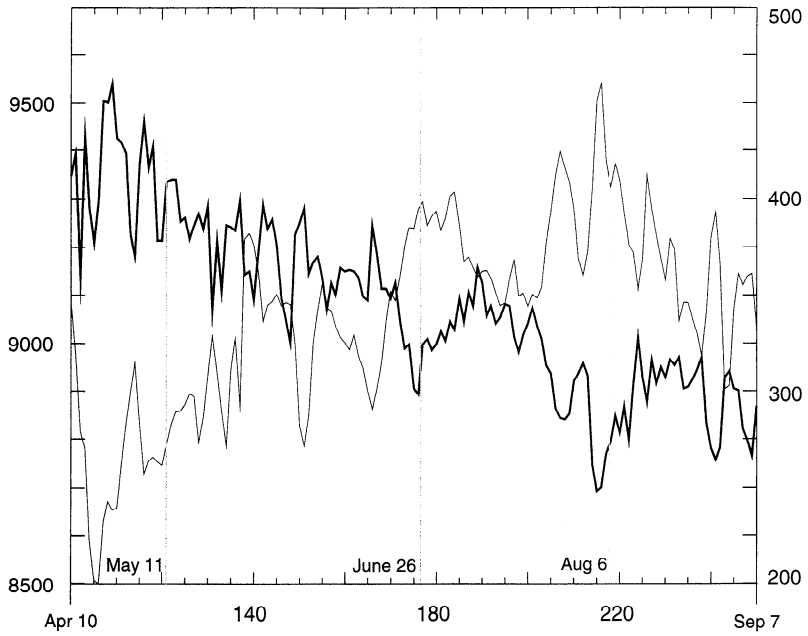

Figure 1. Time series of TOMS column ozone (heavy solid curve, DU on right-hand scale) and ECMWF 300 hPa geopotential height (light solid curve, m on left-hand scale) over Fairbanks, Alaska during the period April 10 to September 7, 1997 (Julian dates 100-250). Vertical lines denote the start of synoptic sequences discussed in sections 4 and 5.

atop the Southeast Asian monsoon, leading to a pronounced maximum in the occurrence of Rossby wave breaking, hence stratosphere-troposphere exchange, downstream over the North Pacific basin. Poleward of the subtropical jet, evanescent synoptic scale waves irreversibly mix the lower stratosphere in tropopause folds described by the classic works of *Danielsen* [1968] and *Shapiro* [1980]. The associated absorption of synoptic wave activity exerts an easterly torque on the zonal mean flow, hence is compatible with a poleward-downward Lagrangian flow. *Holton et al.* [1995] provide a comprehensive summary of stratosphere-troposphere exchange processes.

A mean poleward tropospheric temperature decrease is present at higher northern latitudes all summer, which supports baroclinic growth of synoptic scale disturbances [*Palmen and Newton*, 1961; *Newell et al.*, 1974; *Randel*, 1992]. Rather little is known about their effects on constituent distributions. *Hess and Holton* [1985] and *Hess* [1991] explored mixing processes following the breakup of the winter polar vortex. They found that diabatic processes alter the relationship between potential vorticity (PV) and long-lived trace constituents in late spring and summer, adding to the complexity of the relationship between column ozone and synoptic waves. In this study we use a variety of ozone and meteorological data sets to explore the relationship between ozone and synoptic waves. Case studies confirm that column ozone generally increases (decreases) when downstream of a trough (ridge).

The University of Wisconsin Nonhydrostatic Modeling System (UW-NMS) is used to study a case in May 1997 at mesoscale resolution. NASA's Photochemistry of Ozone Loss in the Arctic Region in Summer (POLARIS) aircraft campaign was carried out between March and September 1997. A goal for our participation in POLARIS was to assess the fidelity of UW-NMS lower stratospheric structures by comparison with balloon and ER2 data. The nonhydrostatic aspect is essential for greater accuracy in representing motions with significant vertical acceleration, a characteristic of mesoscale flows. Our strategy of combining mesoscale dynamical modeling with observationally constrained ozone and idealized tracers is complementary to other modeling techniques, including global models [e.g., *Chipperfield et al.*, 1995; *Douglas et al.*, 1996; *Hansen et al.*, 1997; *Lefevre et al.*, 1998], contour surgery and reverse domain filling [e.g., *Manney et al.*, 1998; *Orsolini et al.*, 1998], and Lagrangian photochemical modeling [e.g., *Bregman et al.*, 1997; *Rex et al.*, 1998].

Section 2 describes the ozone observations, meteorological data, the UW-NMS, and how ozone is initialized. Section 3 describes the ozone profiles and week-to-seasonal variability of ozone and geopotential height over Alaska. Section 4 presents case studies using observations which illustrate how synoptic waves stretch and fold stratospheric and tropospheric air near 300 hPa over Alaska, and modulate column ozone. In section 5 the case study of May 11-12, 1997, is described using POLARIS observations and a UW-NMS simulation. In section 6, consideration of Stokes drift for Rossby waves and a simple box model of ozone transport are used to explore the possibility that net transport out of the po-

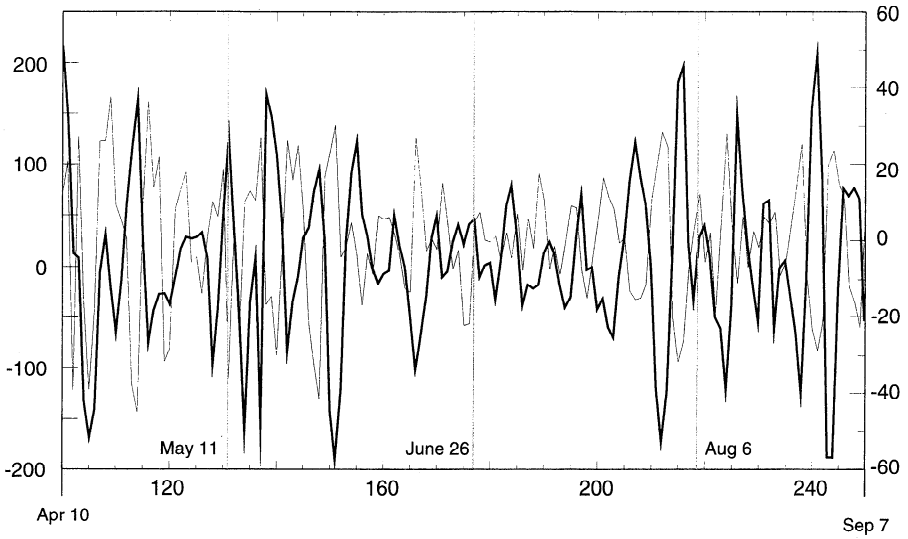

Figure 2. As in Figure 1, except of high-passed time series obtained by subtracting 9 day running mean values from those shown in Figure 1.

lar region contributes to column ozone loss during summer. A discussion and summary are given in section 7.

2. Data and Analysis

2.1 Observations

The NASA POLARIS mission schedule included deployment of the ER2 from Fort Wainwright during phase I (April 30 to May 13), phase II (June 26 to July 11), and phase III (September 5 to 18). Balloon launches occurred regularly throughout the summer, yielding ozone profiles which were used to guide UW-NMS initialization. ER2 and sondes both measured ozone with the dual-beam ultraviolet photometer instrument, which has an accuracy of ~3% or better [*Proffitt and McLaughlin*, 1983; *Proffitt et al.*, 1990].

Daily Total Ozone Mapping Spectrometer (TOMS) column ozone is shown over Fairbanks during April 10 to September 7, 1997 (Figure 1). A high-pass filtered time series (Figure 2) was generated by subtracting a 9-day running mean, emphasizing time scales of days to a week.

Twice-daily gridded analyses of winds, heights, and temperature from the European Centre for Medium-Range Weather Forecasts (ECMWF) were used to investigate synoptic patterns and for initializing the UW-NMS. Details of the properties and limitations of the ECMWF data are given by *Hollingsworth et al.* [1986] and *Trenberth and Olson* [1988].

2.2 UW-NMS

The UW-NMS was designed to study tropospheric scale interaction problems and has been applied to tropical cloud clusters, hurricanes, midlatitude cyclones, polar lows, gravity waves, lake effect snow storms, and mesoscale convective complexes [*Tripoli*, 1992a, b; *Pokrandt et al.*, 1996; *Buker*, 1997; *Jascourt*, 1997; *Mecikalski and Tripoli*, 1997; *Avissar et al.*, 1998]. It includes multiple interactive grid nesting, microphysics, radiative transfer, surface processes, and 1/6° (~18.5 km) resolution topography. Operational tropospheric weather forecasts are available daily on the internet at http://mocha.meteor.wisc.edu.

For application to the polar lower stratosphere, many additional levels were added, with enhanced resolution near the tropopause. For comparison with ER2 data, UW-NMS output is sampled every 60 s. The May 11, 1997 simulation presented in section 5 was initialized from 2.5° ECMWF data and interpolated to a 0.5° grid. The domain is a local spherical grid centered at 160°W, 60°N with a horizontal grid spacing of ~55 km. The domain corners are located at (69.5°N, 223.6°W), (69.5°N, 96.3°W), (37.1°N, 183.2°W), and (37.1°N, 136.8°W), and each side is about 4300 km long. ECMWF data were interpolated to constant altitude surfaces, with vertical resolution varying from 700 m near the surface and model top to 250 m near the tropopause. A 10 grid point Rayleigh friction sponge layer is used to eliminate spurious reflections from the rigid lid at 30 km. Horizontal Rayleigh friction zones along the perimeter extend about 200 km into the interior, with a dissipation time scale of 1.5 hours. The UW-NMS was integrated with a 60 s time step from 0000 UT on May 11, 1997 to 1200 UT on May 12, 1997. The model side walls were updated every hour with temporally interpolated ECMWF data, while the interior was allowed to evolve according to model physics. Model output was archived every 3 hours for history files and every 1/2 hour for making film loops with VIS-5D, freeware which visualizes the temporal evolution of several variables in three dimensions [*Hibbard and Santek*, 1989].

Ozone was initialized in the UW-NMS at and above 100 hPa with data kindly provided by Brad Pierce, Lan-

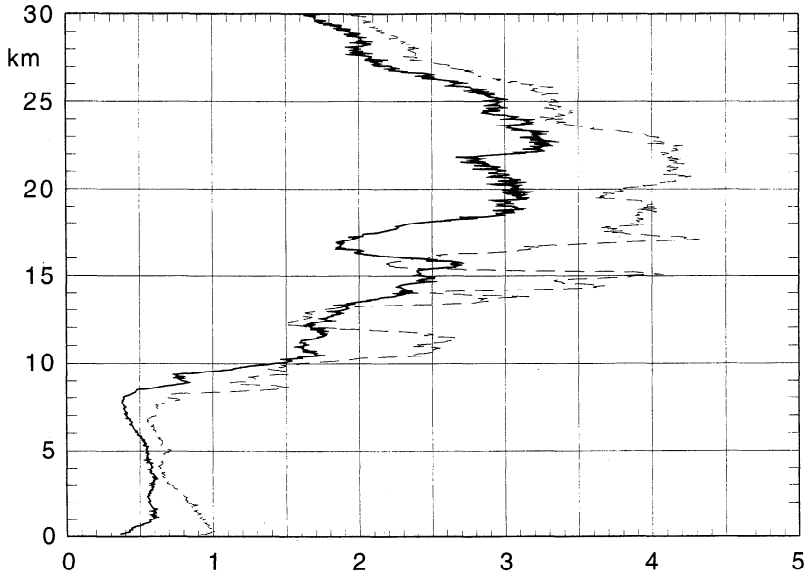

Figure 3. Ozone number density profiles ($10^{18}/m^3$) from balloon flights over Fairbanks on May 11 (dashed curve) and September 30 (solid curve) 1997. Note the decrease in concentration at nearly all levels.

gley Research Center. The method has been adapted from *Schoeberl et al.* [1989] and is described by *Pierce et al.* [1997]. This ozone was created from a Halogen Occultation Experiment (HALOE) methane-potential vorticity (PV) mapping algorithm, where the global coverage and favorable resolution of the United Kingdom Meteorological Office (UKMO) PV distribution is used via correlation with HALOE methane to obtain high resolution methane, and finally regressed on HALOE ozone to obtain globally mapped ozone. Guidance for ozone initialization below 100 hPa was provided by the POLARIS electrochemical concentration cell (ECC) ozonesonde profiles (Figure 3). A constant ozone number density was assumed from the surface to the tropopause, which is taken to be the 1.5×10^{-6} K m^2 s^{-1} kg^{-1} PV unit surface (1.5 PVU). Vertical interpolation is then used between the 1.5 PVU surface and the 100 hPa surface at each horizontal grid point.

Two "ozone" arrays were initialized in the UW-NMS: Tracer 1 is inert ozone, subjected to transport processes alone; tracer 2 is the same, but is set to zero below the 1.5 PVU surface to approximate tropospheric ozone sinks. Difference maps highlight where stratospheric ozone is entering the troposphere. Ozone can be destroyed in the troposphere by contact with the surface, or by reaction with molecules and hydrometeors in the free troposphere. A useful summary of the tropospheric ozone budget is given by *Warneck* [1988, Chapter 5]. *Brasseur et al.* [1999] suggest a tropospheric residence time of ~10 days for ozone in the summer, but the ocean boundary layer is likely to be a strong sink [*Davis et al.*, 1996]. The difference between tracers 1 and 2 may be regarded as an upper bound on irreversible stratosphere-troposphere exchange.

3. Ozone and Height Observations

Figure 1 shows the temporal variation of daily TOMS column ozone (DU) and ECMWF 300 hPa altitude (m) over Fairbanks during April 10 to September 7, 1997 (Julian dates 100-250). The 300 hPa surface (near 9 km) lies near the tropopause, as indicated by the rapid upward increase in ozone seen in Figure 3. From April through early August the 300 hPa height rises from ~8600 to ~9400 m and decreases thereafter, following the seasonal trend in average tropospheric temperature. This rise is irregular, with significant variability at time scales of a week or longer, with amplitudes of ~200 m. Column ozone declined from ~400 DU in early May to ~290 DU in September, a decrease of ~110 DU, and exhibited similar variability with amplitudes of ~30 DU. The correlation coefficient for the two time series in Fig. 1 is -0.78. This correlation improves to -0.86 when a 5 day running mean filter is applied, suggesting that the week to seasonal time scales account for most of the correlation.

The high-passed time series in Figure 2 shows variations at time scales of a week or less. During the data record there were two long periods during which ozone and 300 hPa heights were strongly anticorrelated: days 135-170 and 195-250. At other times phase relationships were less clear. The correlation coefficient for the two time series in Figure 2 is -0.48. This suggests that more of the ozone changes are associated with periods of a week or more, but that the relevant time scales include days to weeks.

Figure 3 shows balloon-borne ECC ozonesonde profiles from Fairbanks, Alaska, on May 11 (Julian date 131, dashed curve) and September 30 (Julian date 273,

solid curve). Both profiles exhibit considerable vertical layering at many scales. The pronounced minimum near 16 km in the May 11 profile was sampled by the ER2. Note that each 5 km x 10^{18} m^{-3} square in Figure 2 represents $5x10^{21}$ ozone molecules m^{-2}, or a ~20 DU column contribution. An areal estimate suggests an ozone reduction between these two times of ~45 DU in the layer 8-16 km, and of ~110 DU in the layer 8-25 km.

4. Synoptic Patterns and Ozone

Inspection of daily synoptic charts for the summer of 1997 reveals that marked disturbances exist which move rather slowly, with periods exceeding a week. Synoptic sequences are shown first for two periods of rising column ozone (June 26 to July 8 and August 3 to 13), then for the May 11-12 case study. The 300 hPa surface is chosen for emphasis since the axis of maximum flow speed and dynamical tropopause intersect this surface near Alaska, separating stratospheric air to the north from tropospheric air to the south.

Figure 4 shows a sequence of 300 hPa heights and winds on June 26 (Julian date 177), July 1 (182), and July 8 (189), 1997. June 26 is indicated by a thin vertical line in Figure 1. During this time, column ozone over Fairbanks increased from 320 to 350 DU, while the 300 hPa height decreased from 9300 m to 9150 m, changes of +30 DU and -150 m. On June 26 a high pressure system dominated northern Alaska, extending westward toward the north Siberian coast (Figure 4a). The low height center in the eastern Pacific is nearly in a blocking configuration with the high over Alaska. Two troughs were located upstream, one near Kamchatka and another over the Arctic Ocean north of Siberia.

Five days later (July 1) one can see that the trough over the Arctic Ocean has propagated eastward and is located north of Alaska (Figure 4b). The high over Alaska has weakened and moved eastward. By July 8 (Figure 4c) the low pressure center was seated in the Gulf of Alaska, and the Arctic Ocean trough had moved farther east and amplified considerably. Figure 5 shows UW-NMS ozone at 10 km on July 1, together with 6 day back trajectories from near Fairbanks. Air arriving over Fairbanks circulated through the trough, which contains enhanced ozone (compare Figures 5 and 4b). During this period the Alaska high pressure system has been entirely displaced by a westerly flow through the trough, advecting in polar stratospheric air with high PV and high ozone.

The passage of this Arctic trough marked the beginning of a long period of declining column ozone (Figure 1, after day 189). Near August 3, 300 hPa heights reached their highest value of the summer over Fairbanks, ~9550 m, while column ozone reached its lowest value, ~250 DU. On August 6 a pronounced ridge extended up the west coast of North America into Alaska (Figure 6a). Back trajectories (not shown) suggest that some of the air reaching Fairbanks arrived by way of the midlatitude Pacific. A week later (Figure 6b) the high had retreated southward over the northeastern Pacific, leaving a trough to dominate the flow upstream of Fair-

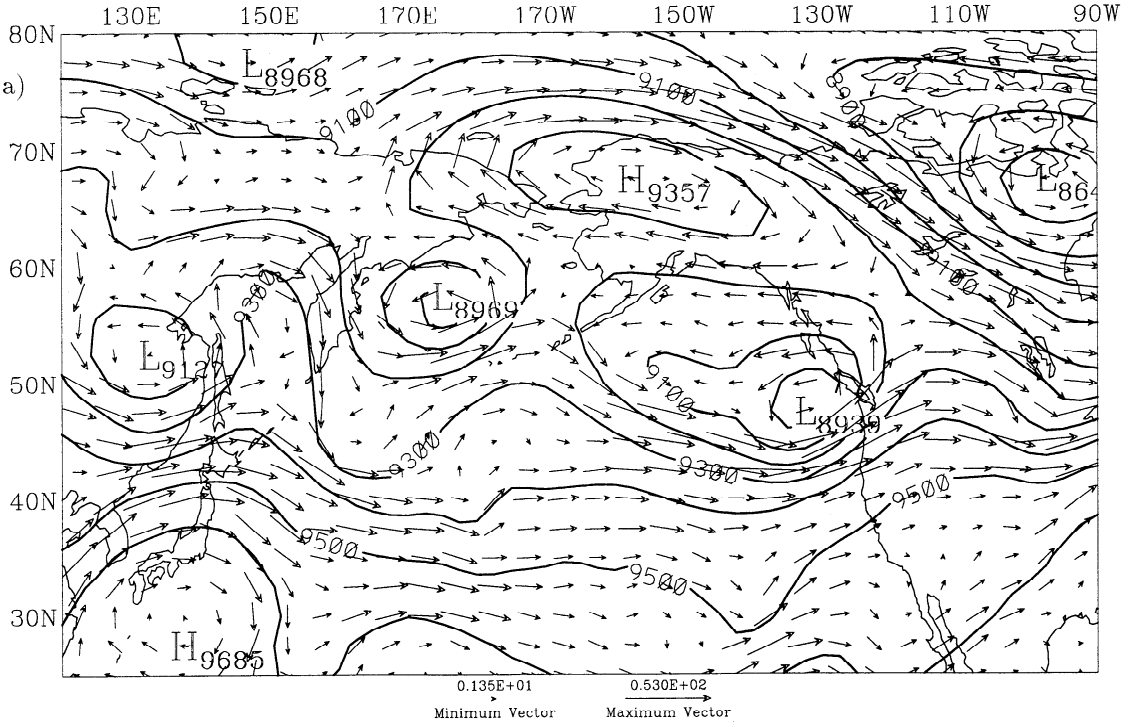

Figure 4. ECMWF 300 hPa horizontal winds and heights at (a) 0000 UT June 26, 1997 (177), and (b) 1200 UT July 1, 1997 (182), 0000 UT July 8, 1997 (189). The trough at the northern edge travels eastward at ~3 m/s as ozone rises by 30 DU.

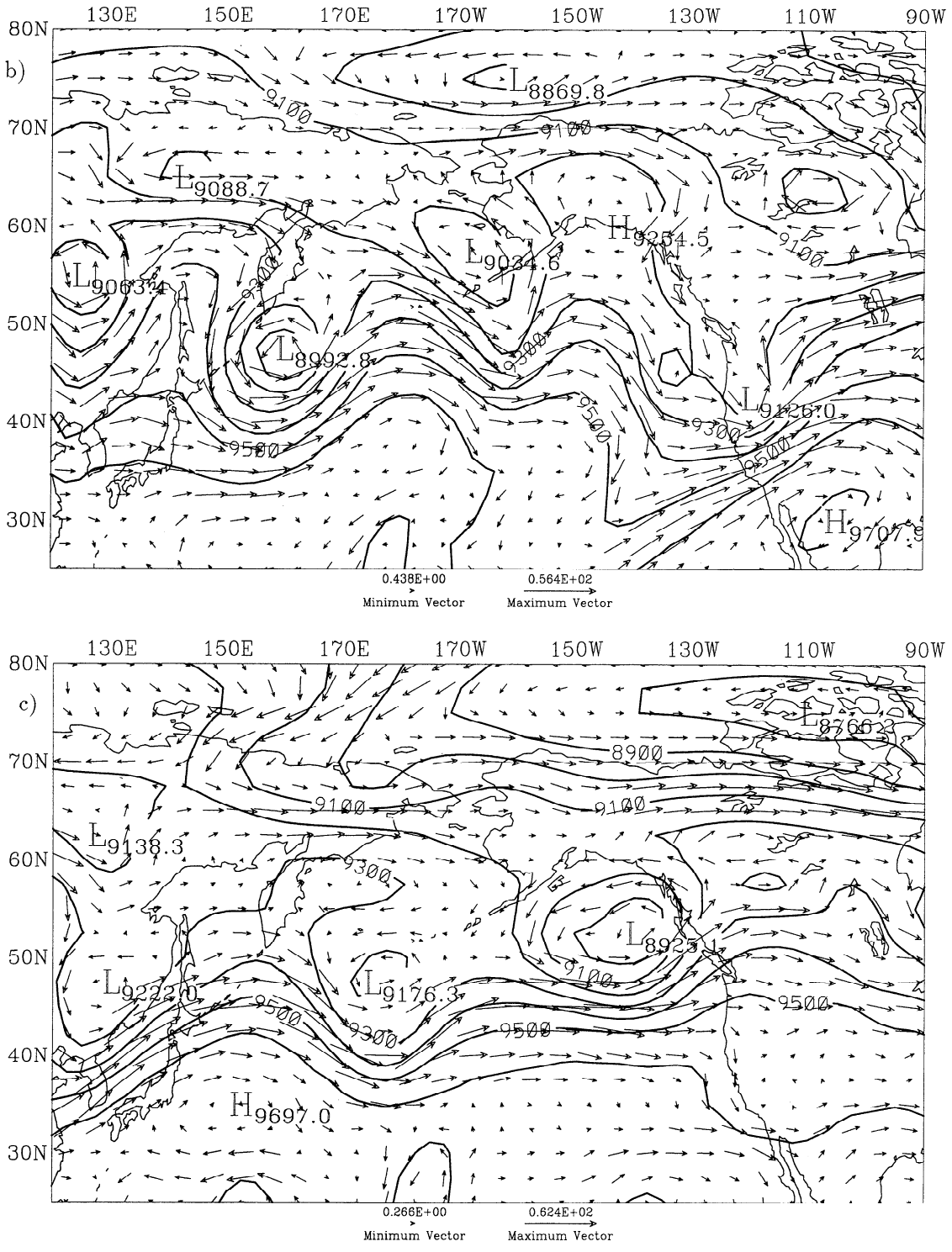

Figure 4. (continued)

banks. Trajectories arriving over Alaska on August 13 originated primarily over Siberia (not shown). During this time column ozone rose from 250 to 310 DU, an increase of 60 DU (Figure 1).

Figure 7 shows 300 hPa heights and winds at 0000 UT on May 11 and 13 (days 131 and 133). On May 11 (Figure 7a) a zonally oriented trough extended from Siberia to the Bering Sea. A meridionally elongated trough is seen south of Alaska near 150°W, with a characteristic zonal wavelength of ~3000 km. By May 13 (Figure 7b) the digging trough had rolled up into a closed vortex off the coast of California.

This period was of particular interest because of the frequent sampling by ER2 and balloon flights, and the opportunity to study the "G cleff" signature in PV and ozone, associated with the type 1 life cycle for baro-

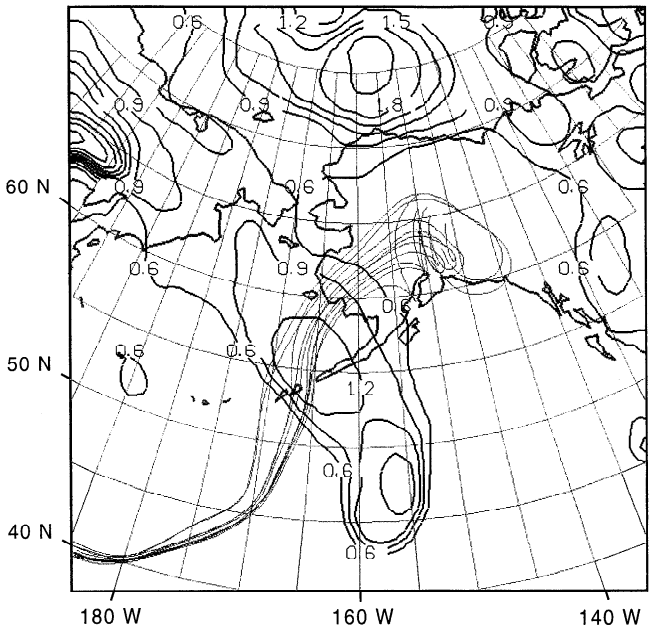

Figure 5. Ozone (contour interval 0.3 ppmv) and 6 day back trajectories at 10 km on July 1, 1997.

clinic waves ("LC1") [*Thorncroft et al.*, 1993]. The LC1 is characterized by a thinning trough, seen as a stratospheric PV filament near the tropopause, that penetrates equatorward and bends anticyclonically. This usually leads to cyclonic vortex roll-up and the formation of a cutoff low [*Hoskins et al.*, 1985]. In the eastern Pacific this is often followed by amplification of a blocking high pattern [*DePondeca et al.*, 1998]. Note that during the week following May 13, column ozone declined and heights rose (Figure 1). UW-NMS results in the next section suggest that this stratospheric vortex filament is a site of vigorous stratosphere-troposphere exchange.

5. Case Study of May 11-12

5.1. UW-NMS Simulation

The model domain, sea level pressure, streamfunction at 14 km, and the location of the 7 PVU surface are shown for 1200 UT May 11, 1997 in Figure 8, 12 hours after initialization. Surface lows over the Bering Sea and Gulf of Alaska coincide with downward excursions of the 7 PVU surface (Figure 8) and low 300 hPa heights (Figure 7a). Figure 9 shows a plan view of PV at 10 km, confirming that both troughs are fairly barotropic. The elongated stratospheric PV filament, however, has only a weak surface low associated with it, while that in the Bering Sea is quite robust.

The diagonal line in Figure 9 shows the location of the vertical section through the Bering Sea and Gulf of Alaska troughs shown in Figures 10, 11, and 14. Figure 10 shows p'^2/ρ, a measure of synoptic wave activity, where p' is the deviation from the domain average pressure at a given altitude and ρ is density. (A measure of synoptic wave activity may be taken to be $\rho\psi'^2$, where ψ' is the geostrophic streamfunction, which is related to geopotential height by $\psi' = gZ'/f$, where f is the Coriolis parameter. Using the hydrostatic law, $\partial p' = -\rho g \partial Z'$, $\rho\psi'^2 \propto p'^2/\rho$.) The lower stratosphere exhibits significant synoptic wave activity to at least 14 km. The heavy dashed line (1.5 PV surface) indicates the local tropopause. The summertime disturbances tend to have maximum pressure amplitudes near the tropopause. From Figure 10 one may estimate that p' exceeded 30 hPa over the Bering Sea, but is ~10 hPa in the filament. Although the PV values are larger in the LC1 filament, associated pressure perturbations are weaker than in the Bering Sea trough.

The UW-NMS creates mesoscale structures from initialized coarser data in accordance with model physics. Figure 11 shows a vertical section of model streamfunction and ozone mixing ratio (gray) on May 11, as seen from the northeast. Near 10 km, stratospheric ozone (gray, Figure 11) extends downward with the 1.5 PVU surface (Figure 10) over both lows. Much of this ozone structure was present in the initialized HALOE ozone field, but features evolved and sharpened during model integration. The model circulation in this plane is consistent with stratospheric air entering the troposphere near the Bering Sea. Near the Gulf of Alaska stratospheric filament the relationship between streamfunction and ozone appears to be more complex and requires further study.

The synoptic charts and this meridional streamfunction pattern suggest a rich array of stretching and folding: vertical overturning, confluence, and difluence, the hallmarks of mixing [e.g., *Duan and Wiggins*, 1996; *Ngan and Shepherd*, 1997]. An example of pronounced horizontal difluence approaching the high PV filament is shown in Figure 9. The gray region is a 65 m/s isotach at 1200 UT on May 12. During 24 hours, air parcels near this polar jet traveled more than 1000 km eastward and diverged meridionally approaching the high PV filament. Rapid separation of upstream air parcels is a significant component of these stratospheric LC1 filaments. On the eastern side of the filament a similar difluent trajectory pattern occurs in the lower stratosphere and upper troposphere north of an occlusion (not shown), in association with the development of an isobaric thermal ridge, a feature known as a "trowal", or trough of warm air aloft [*Martin*, 1999]. Some of this upper tropospheric air to the east of the filament has its origin in the lower tropospheric warm sector (not shown). The tropopausal PV filament is a location where parcels of disparate origin are brought closer together.

5.2. Comparison With ER2 data

Model column ozone at 1200 UT on May 11 is shown in Figure 12a. Values exceeding 470 DU and 8 PVU (Figure 9) are seen in the Bering Sea trough and in the stratospheric vortex filament. Near Fairbanks, modeled column ozone is ~440 DU, ~20 DU higher than TOMS column ozone (Figure 1). Some differences in column

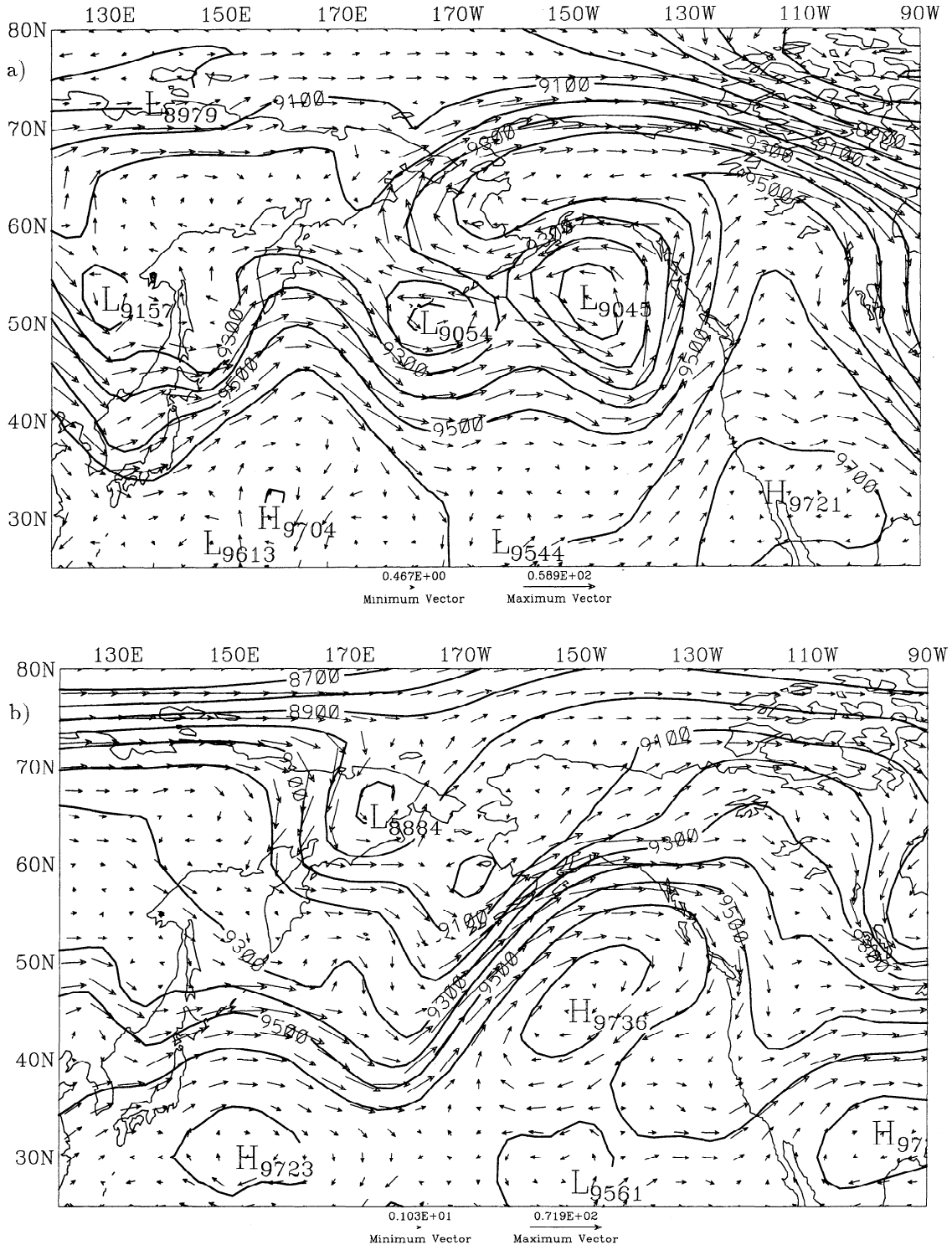

Figure 6. ECMWF 300 hPa winds and heights near (a) the beginning, 0000 UT August 6, 1997 (218) and (b) end, 1200 UT August 13, 1997 (225) of an ozone rise of 40 DU.

ozone are to be expected due to the challenge of specifying horizontal variations of ozone below 100 hPa in the UW-NMS. Column ozone increases moderately toward the southwest from Fairbanks.

The ER2 flew in a stacked pattern on May 11. The projections of the flight path in longitude-latitude and longitude-altitude are shown in Figures 12a and 12b. The northeast-southwest oriented flight spanned 150°-144°W, 61.5°-65°N, and the layer 8-21 km, affording a stringent test of UW-NMS ozone fidelity. Figure 13 shows the ER2 altitude (thin stairstep curve), ER2 ozone mixing ratio (thin solid curve), and UW-NMS ozone mixing ratio (thin dashed curve). Considering the strong vertical ozone variations seen in Fig. 3, agree-

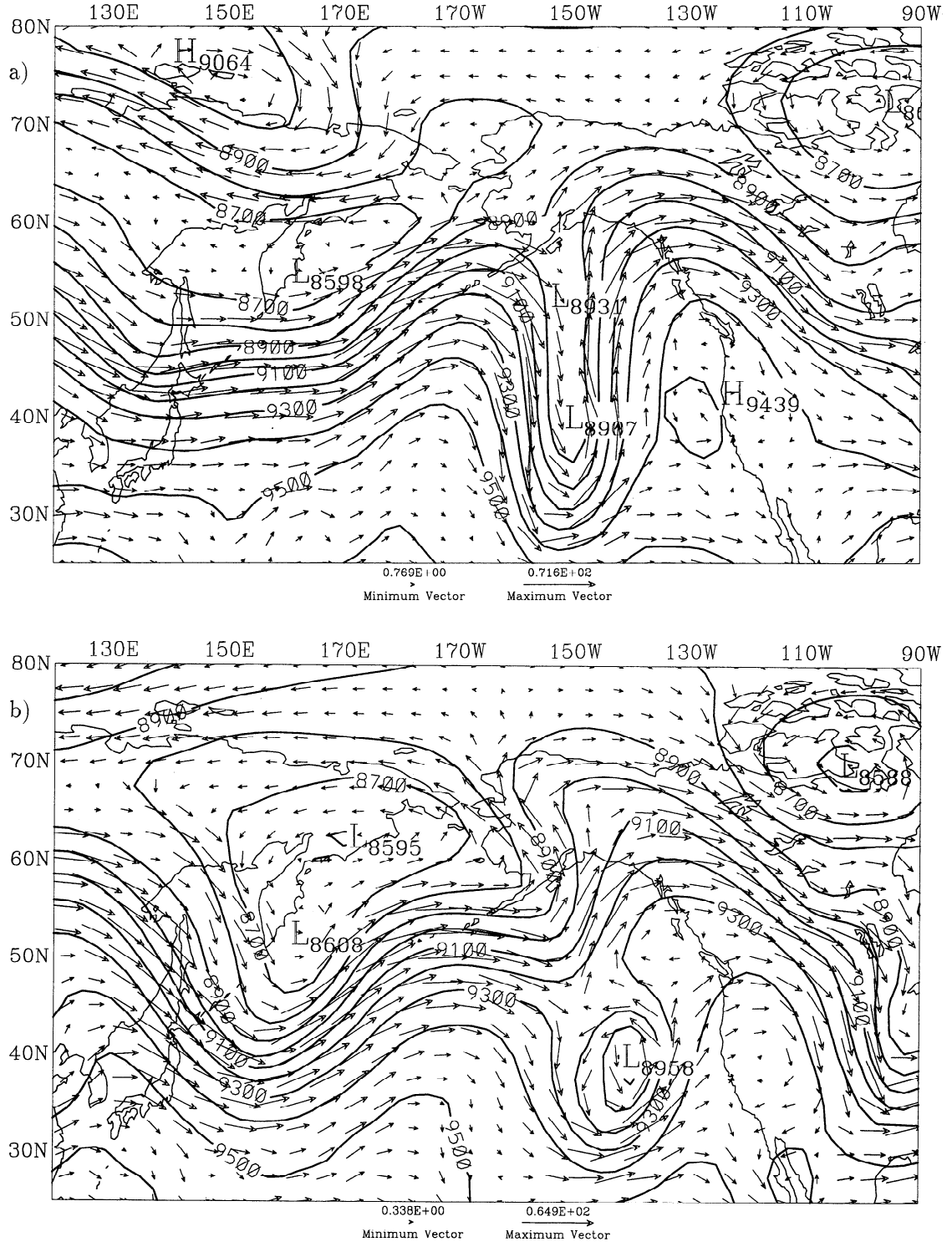

Figure 7. ECMWF 300 hPa heights and winds at 0000 UT on (a) May 11, and (b) May 13, 1997.

ment between the ER2 and the UW-NMS ozone fields is fairly good. An exception is the northeastward leg near 15 km starting at 81,000 s, where modeled ozone is clearly too high relative to ER2 observations. The ozone profile in Figure 3 shows a 50% decrease from 15 to 16 km. The ER2 sampled the minimum near 16 km, while the flight track in the UW-NMS sampled a layer of higher ozone. This discrepancy is likely due to vertical grid spacing in the model.

5.3. UW-NMS Ozone

Figure 14a shows a section of UW-NMS ozone volume mixing ratio (tracer 1) at the end of the model run, along the curve shown in Figure 9. This view from the southwest is complementary to Figures 10 and 11. It supports the idea that stratospheric air is entering the troposphere in the Bering Sea low and near the PV filament in the Gulf of Alaska. Recall that tracer 1 is

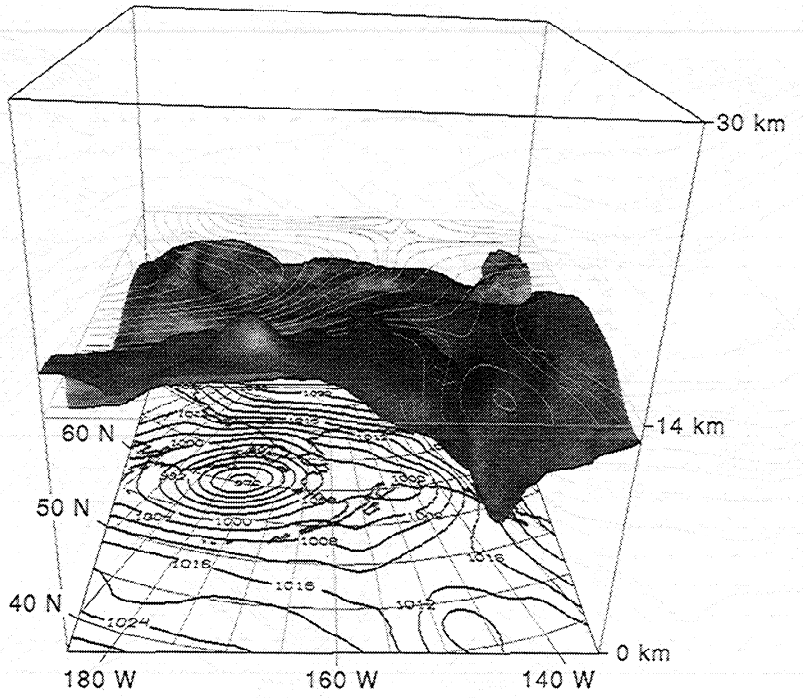

Figure 8. UW-NMS model domain, sea level pressure (contour interval 4 hPa), and streamfunction on the 7 PVU surface at 1200 UT on May 11, 1997, after 12 hours of integration.

conserved following model initialization, but tracer 2 is set to zero below the 1.5 PV surface. The difference section, tracer 1 minus tracer 2, is shown in Figure 14b. In the stratosphere both tracers are identical, so their difference is near zero. The difference increases downward into the troposphere, where typical values are 0.3 ppmv for tracer 1, but are zero for tracer 2. The transition zone occupied by contours exists because some ozone has descended through the tropopause, where it is set to zero for tracer 2, but not for tracer 1. In the UW-NMS, irreversible processes, including radiation, advected turbulent kinetic energy, and numerical effects, can alter the relationship between tracer and PV patterns. The area occupied by contours is largest near the PV filament, suggesting that it is an active site of stratosphere troposphere exchange.

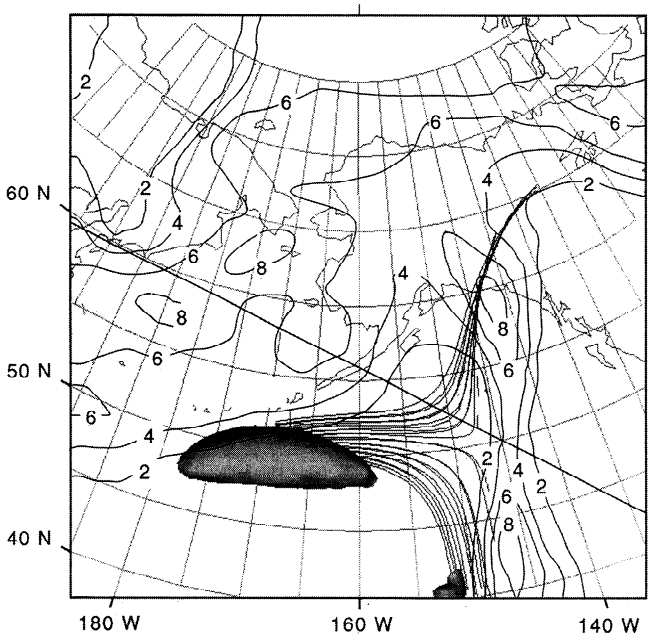

Figure 9. UW-NMS PV (contour interval 2 PVU) at 10 km, 1200 UT on May 11, 1997. Trajectories were integrated forward for 24 hours from near the jet maximum to the west (shown by the 65 m/s isotach surface in gray). The diagonal line shows the location of vertical cross sections in Figures 10, 11 and 14.

6. Transport by Synoptic Waves

6.1. Stokes Drift Due to Synoptic Waves

Wallace [1978] argued that in synoptic waves near the tropopause, ascent tends to occur just downstream of the maximum northward flow, while descent occurs just downstream of southward flow. As a consequence, parcel motions will execute counterclockwise trajectories in latitude-altitude, with the north pole to the right [e.g., *Kida*, 1977, Figure 12]. Owing to the decrease of wave amplitude away from the subtropical tropopause, trajectories are not closed, yielding a Stokes drift which is poleward and downward. Here a simple derivation of the Lagrangian flow is given which illustrates the dependence on the gradient of wave variance and on the phase relationship between v' and w'.

Let an idealized perturbation streamfunction be represented as

$$\psi' = \hat{\psi}(y, z)\cos(kx - \omega t), \quad (1)$$

where $\hat{\psi}^2(y, z)$ decreases away from the location of maximum amplitude. The rotational meridional eddy flow

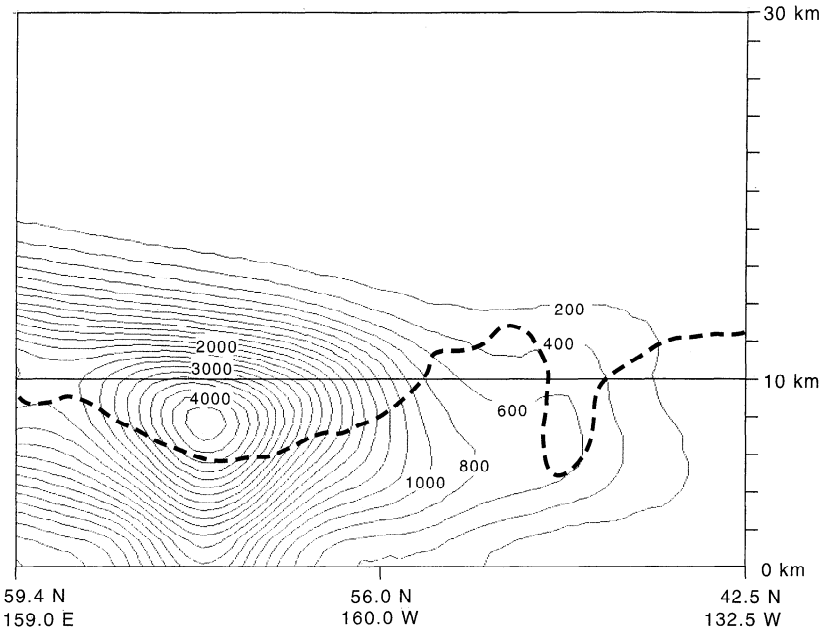

Figure 10. Section of p'^2/ρ in the UW-NMS on May 11, 1997, along the diagonal line shown in Figure 9 (contour interval 200 Pa). The heavy dashed curve is the 1.5 PVU contour, an indicator of the tropopause.

is then

$$v' = \frac{\partial \psi'}{\partial x} = -k\ \hat{\psi}\ \sin(kx - \omega t) \quad (2)$$

Observe that w' and v' patterns will be similar, but with a phase shift δ and amplitude factor α (which is negative in the southern hemisphere to account for the "poleward-upward" relationship between v' and w' in baroclinic waves):

$$w' = -\alpha\ k\hat{\psi}\ \sin(kx - \omega t + \delta)\ . \quad (3)$$

Following *Andrews et al.* [1987, equation (4.5.25)], the Stokes drift due to eddies is estimated from

$$\overline{v}^L = \frac{\partial \overline{\eta v}}{\partial y} + \frac{\partial \overline{\zeta v}}{\partial z}\ , \qquad \overline{w}^L = \frac{\partial \overline{\eta w}}{\partial y} + \frac{\partial \overline{\zeta w}}{\partial z}\ , \quad (4)$$

where η and ζ are meridional and vertical parcel displacements. Integrating (2) and (3) in time to obtain η and ζ, and averaging in time over a cycle or more, it is readily shown that (4) becomes

$$\overline{v}^L = -\gamma\ \sin\delta\ \frac{\partial}{\partial z}\hat{\psi}^2\ , \qquad \overline{w}^L = \gamma\ \sin\delta\ \frac{\partial}{\partial y}\hat{\psi}^2\ , \quad (5)$$

where $\gamma = \alpha k^2/(2\omega)$. Above the upper tropospheric amplitude maximum, $\partial\hat{\psi}^2/\partial z < 0$, while poleward of this maximum, $\partial\hat{\psi}^2/\partial y < 0$. Thus, for $\delta > 0$, the Lagrangian flow is expected to be poleward and downward in the polar lower stratosphere. A phase shift $\delta > 0$ corresponds to upward motion occurring downstream of the northward flow maximum. In the UW-NMS, w' tends to maximize just downstream of v' maxima (not shown), although synoptic patterns are much more complex than simply sinusoidal.

6.2. Box Model of Polar Ozone

Consider a highly idealized version of the stratosphere, where polar air is distinguished from tropical air. Following seminal work on tropical - extratropical exchange [e.g., *Volk et al.*, 1996; *Avallone and Prather*, 1996; *Minschwaner et al.*, 1996; *Mote et al.*, 1999], consider stratospheric transport between the tropics and polar regions as having a mixing time scale τ_{in}, and a descent rate w out of the bottom of the polar box. Let us hypothesize, following *Kida* [1977] and *Wallace* [1978], that these waves induce a Lagrangian descent poleward of the wave amplitude maximum. Net radiative heating provides a useful measure of how fast the air is rising or sinking. Lagrangian parcel trajectories through synoptic waves lead to large temperature excursions and enhanced wave absorption by infrared relaxation. Irreversible transport is intimately related to wave absorption. Assuming that diabatic cooling is ~ -0.5 K/d, descent should occur at ~1 km/10 d. From Figure 3, a descent of 9 km in 3 months equals six boxes, or 120 DU of ozone. Ozone likely flows out the base of the stratosphere all summer through a deep layer.

The conservation equation for ozone volume mixing ratio r is $dr/dt = S_r$. While the source/sink term is clearly of interest, here we investigate the net effect of meridional transport between the polar and midlatitude boxes, and descent through the bottom of the polar stratospheric box:

$$\frac{\partial r_p}{\partial t} = -w\frac{\partial r_p}{\partial z} - \frac{(r_p - r_m)}{\tau_{in}}\ , \quad (6)$$

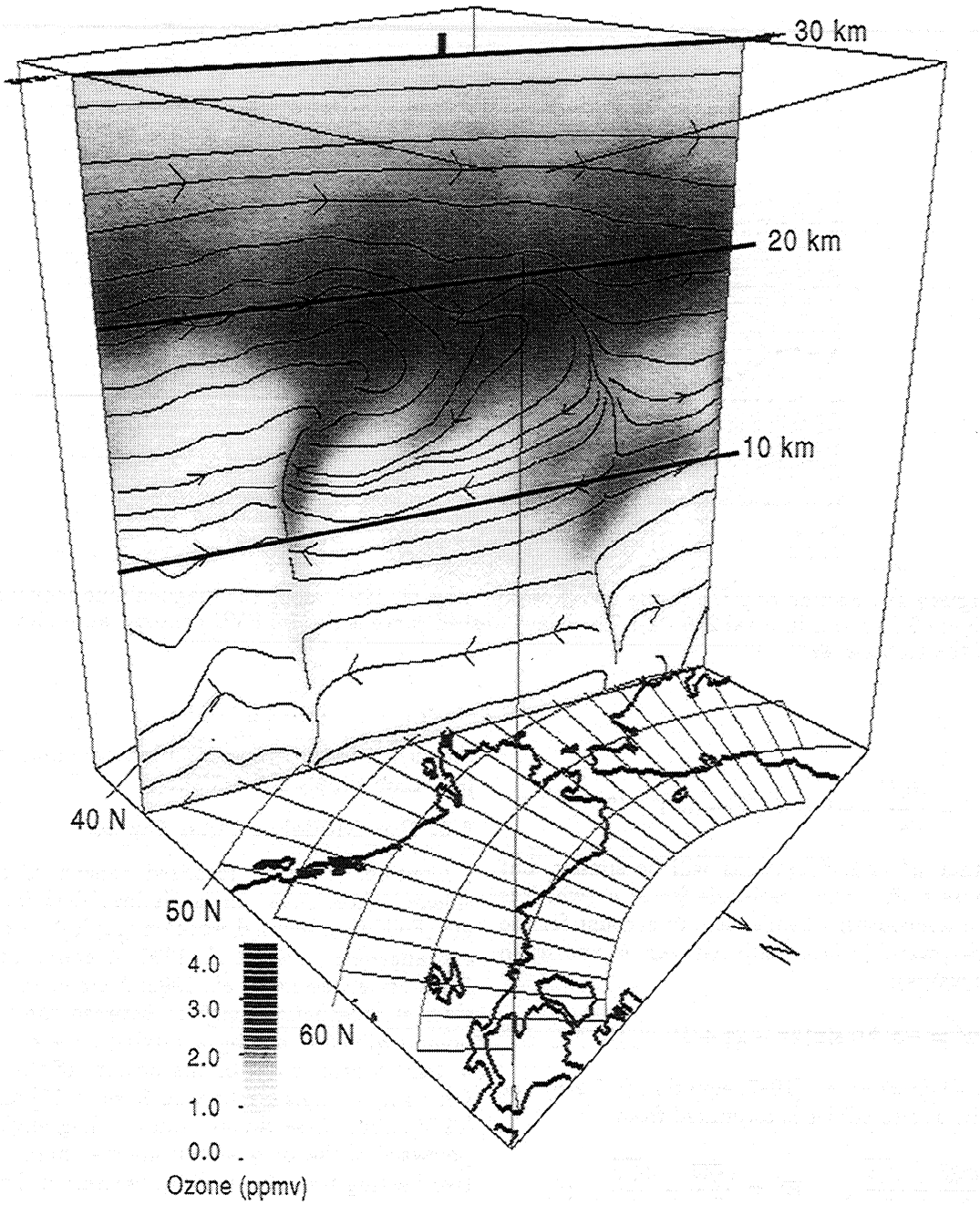

Figure 11. Meridional section of streamfunction and ozone (stratospheric values in dark gray) in the UW-NMS on May 11, 1997, along the diagonal line shown in Figure 9.

where $(r_p - r_m)$ is polar minus midlatitude ozone mixing ratio. From Figure 3, a reasonable vertical scale for ozone variation is ~10 km, so that $\partial r_p/\partial z \sim r_p/10$ km. Near the spring polar ozone maximum the time derivative in (6) is zero. If it is assumed that $(r_p - r_m) \sim -r_p/2$, then $\tau_{in} \sim 50$ days, suggesting that it takes about a season to build up ozone during winter.

In the summer, the mid and upper stratospheric planetary wave transport of ozone out of the tropics is reduced considerably relative to the winter and spring. By examining seasonal mean ozone distributions [e.g., *Andrews et al.*, 1987, Figure 10.4], seasonal changes in the difference in ozone mixing ratio between high and low latitudes are not very noticeable, nor are seasonal changes in vertical gradients near the base of the stratosphere (Figure 3). If we assume that τ_{in} ~100 days in the summer, but keep the descent rate and ozone gradients the same, then

$$\frac{1}{r_p}\frac{\partial r_p}{\partial t} = \frac{-1\text{ km}}{(10\text{ d})(10\text{ km})} + \frac{1}{2}\frac{1}{(100\text{ d})} = -\frac{1}{200\text{ d}}. \quad (7)$$

In 4 months an initial amount of ozone could decrease by 45% according to this simple model, supporting the

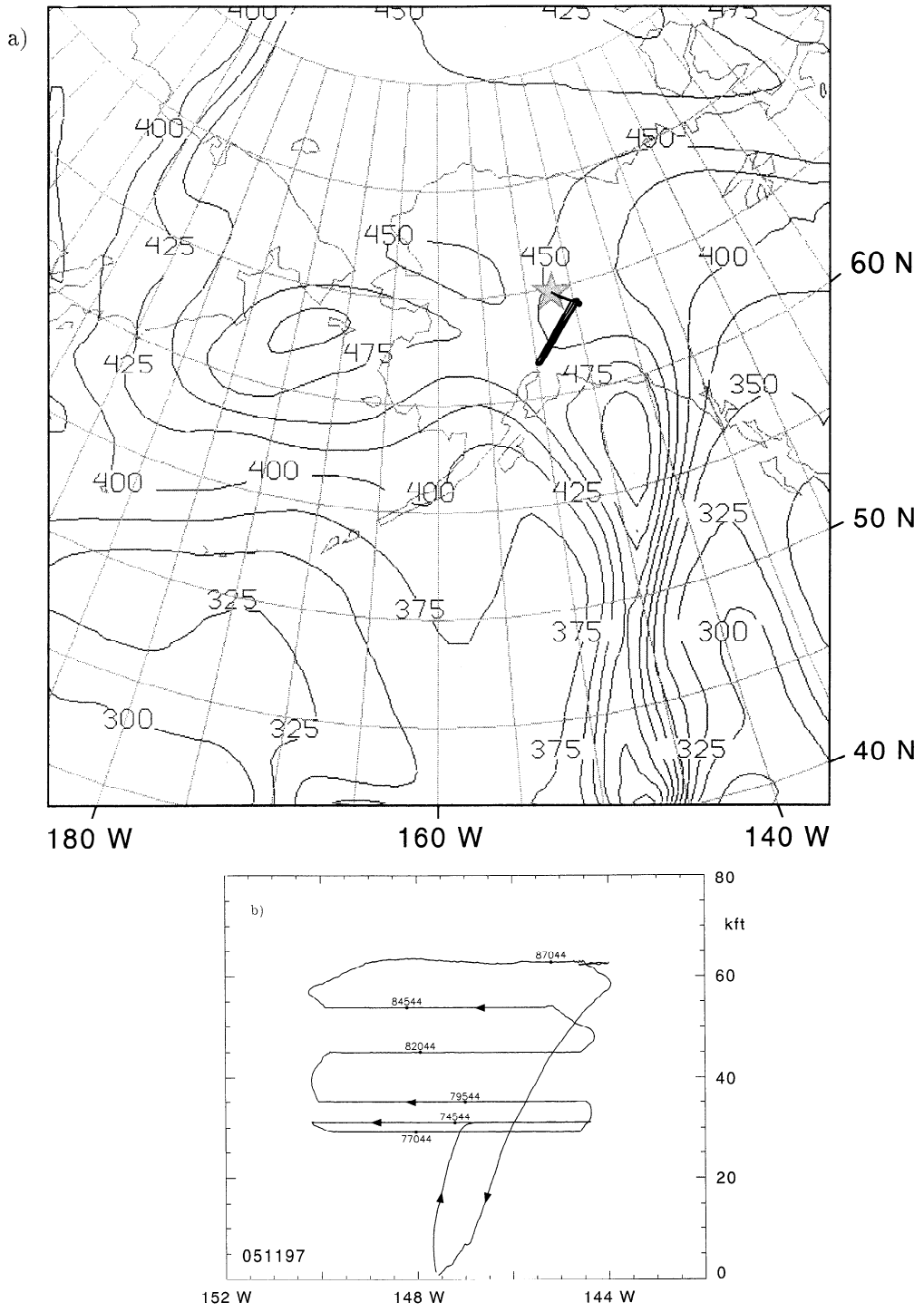

Figure 12. (a) UW-NMS column ozone on May 11, 1997, with a plan view of the ER2 "stacked flight" superimposed, and (b) the flight track in longitude-latitude, with altitude labeled in thousands of feet (kft). Local times of day are given along the flight track in seconds.

idea that a seasonal change in net transport (reduced import from the tropics aloft) is important to consider in working toward a quantitative understanding of summertime column ozone loss.

7. Summary

Across the boreal summer of 1997, column ozone declined while the thickness of the troposphere increased. A rise of the tropopause may be anticipated with increased mixing by baroclinic disturbances and deep convection. The inverse relationship between ozone and 300 hPa height on weekly and longer time scales is quite striking, with correlation coefficient ~-0.8. In general, a change of 10 DU corresponds to a 300 hPa change of 50 m (in the opposite sense).

Three examples of synoptic sequences were used to illustrate the patterns which accompany column ozone

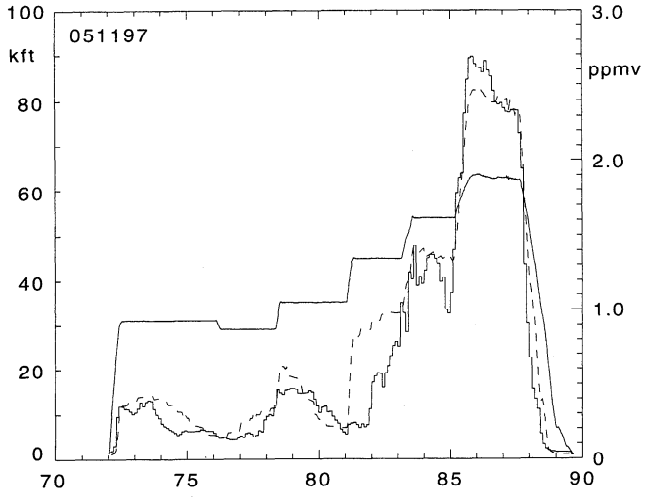

Figure 13. ER2 altitude (thin solid stairstep, thousands of feet (kft), left axis) and ozone (solid, ppmv, right axis) for the May 11, 1997 flight, together with UW-NMS model ozone (thin dashed curve) along the flight track.

increase and decrease. Synoptic scale waves noticeably disturb ozone from the near the tropopause to at least 15 km altitude. When Fairbanks is downstream of a long trough, ozone descends out of the stratospheric trough and is advected over Fairbanks. Conversely, when a ridge exists upstream, low PV tropical air prevails, which displaces high-ozone air. The transient three dimensional motion associated with these synoptic waves facilitates a net descent of stratospheric air into the troposphere compatible with a net cooling rate of ~0.5 K/d. This flow into the polar troposphere likely persists all year long. It is an important component of the column ozone budget for both winter accumulation and the summer diminution.

A box model illustrates the possibility that persistent removal of ozone downward throughout the summer is no longer balanced by import from low latitudes by the large stratospheric waves which existed in the wintertime. The UW-NMS ozone experiments, while strongly suggestive of irreversible intrusion of ozone into the troposphere in association with the synoptic eddies, must be regarded as preliminary. We are in the process of carrying out a detailed ozone budget for the UW-NMS domain to quantify the contribution of net transport to summertime column ozone loss. Primary sources of uncertainty include fluxes through the UW-NMS boundaries and ozone initialization in the troposphere.

The pronounced meridional folding of stratospheric and tropospheric air is an essential ingredient in irreversible mixing of air masses to small scale. *Morgan and Nielsen-Gammon* [1998] explored the interrelationship among tropopausal PV, upper level troughs, and tropopause folding. Recently, *Langford and Reid* [1998] have used ground-based lidar observations to investigate the effectiveness of small-scale processes in irreversible transfer of stratospheric air into the upper troposphere. The characteristic slow propagation speed of the summertime synoptic waves may be regarded as a consequence of modest mean westerly winds and, due to the smallness of the planetary vorticity gradient at high latitudes, an upstream Rossby wave propagation velocity of less than 1 m/s. It is of interest to compare the properties of the Bering Sea and Gulf of Alaska troughs during the May case study. Both have similar PV values, but the arrangement is circular over the Bering Sea

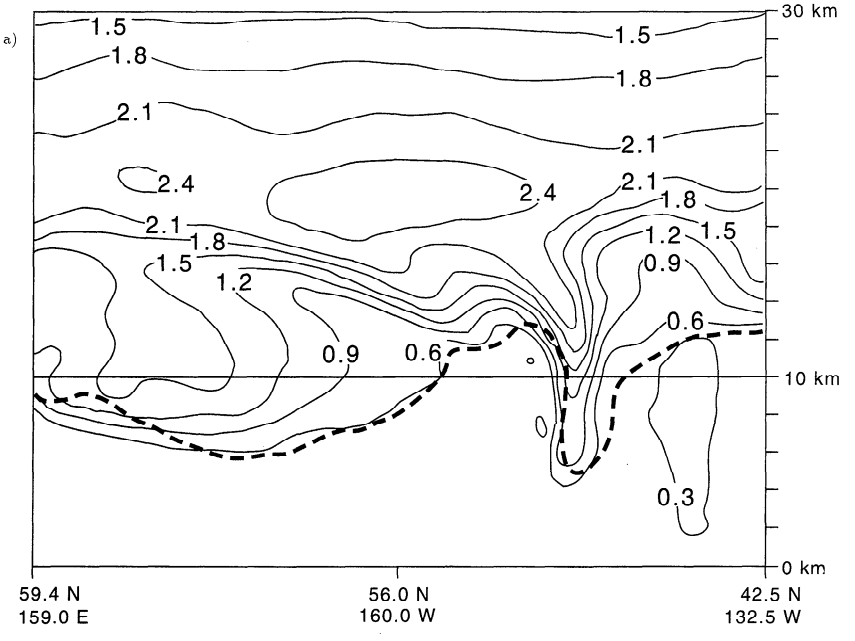

Figure 14. Cross sections of UW-NMS ozone and the 1.5 PVU contour (dashed line) at 1200 UT May 12, 1997 along the curve shown in Figure 9: (a) tracer 1, which is inert after initialization, and (b) tracer 1 minus tracer 2, where tracer 2 is set to zero below the 1.5 PV contour.

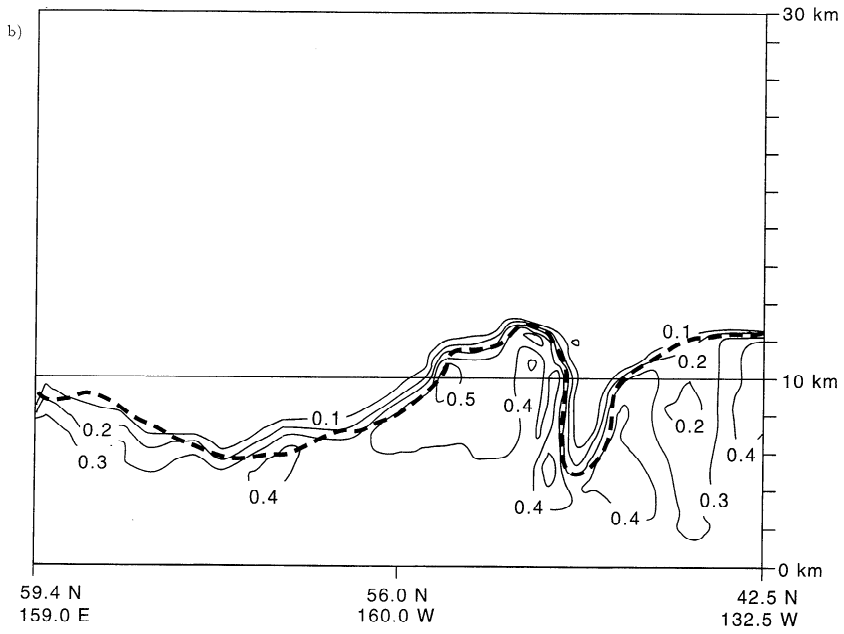

Figure 14. (continued).

and linear in the Gulf of Alaska. The pressure perturbations were much smaller at all levels in the LC1 filament, but the UW-NMS experiment suggested that this filament is a very active site of stratosphere-troposphere exchange. This may be related to the smaller spatial scale of the filament relative to the Bering Sea low.

Acknowledgments. We are grateful to the POLARIS science team for providing data used in this work. POLARIS data may be accessed by contacting Steve Gaines at gaines@cloud1.arc.nasa.gov. We thank Brad Pierce for kindly providing the HALOE-PV mapped ozone for initializing the UW-NMS. We acknowledge useful conversations with Lynn Harvey, Jon Martin, Michael Morgan, and Greg Postel, and thank the reviewers for their suggestions. Steve Lloyd first called our attention to the week-to-week synoptic ozone variations. This work was supported by the National Aeronautics and Space Administration under a SAGE II Science Team grant, NAS1-96030.

References

Andrews, D. G., J. R. Holton, and C. B. Leovy, *Middle Atmosphere Dynamics*, 489 pp., Academic, San Diego, Calif., 1987.

Avallone, L. M., and M. J. Prather, Photochemical evolution of ozone in the lower tropical stratosphere, *J. Geophys. Res.*, *101*, 1457-1461, 1996.

Avissar, R., E. Eloranta, K. Gurer, and G. J. Tripoli, An evaluation of the large eddy simulation option of the Regional Atmospheric Modeling System in simulating the convective boundary layer: A Fife case study, *J. Atmos. Sci.*, *55*, 1109-1130, 1998.

Bojkov, R., Ozone variations in the northern polar region, *Meteorol. Atmos. Phys.*, *38*, 117-130, 1988.

Brasseur, G. P., J. J. Orlando, and G. S. Tyndall (Eds.), *Atmospheric Chemistry and Global Change*, 654 pp., Oxford Univ. Press, New York, 1999.

Bregman, A., et al., Ozone depletion in the late winter lower Arctic stratosphere: Observations and model results, *J. Geophys. Res.*, *102*, 10,815-10,828, 1997.

Brewer, A. W., Evidence for a world circulation provided by the measurements of helium and water vapor distribution in the stratosphere, *Q. J. R. Meteorol. Soc.*, *75*, 351-363, 1949.

Buker, M. L., Nonhydrostatic modeling of gravity waves and tracer transport in the tropical lower stratosphere: First results, M.S. thesis, 95 pp., Univ. of Wis.-Madison, 1997.

Carlslaw, K. S., et al., Particle microphysics and chemistry in remotely observed mountain polar stratospheric clouds, *J. Geophys. Res.*, *103*, 5785-5796, 1998.

Chipperfield, M. P., et al., The variability of $ClONO_2$ and HNO_3 in the Arctic polar vortex: Comparison of sounding measurements and three-dimensional model results, *J. Geophys. Res.*, *100*, 9115-9129, 1995.

Danielsen, E. F., Stratospheric-tropospheric exchange based upon radioactivity, ozone, and potential vorticity, *J. Atmos. Sci.*, *25*, 502-518, 1968.

Davies, W. E., G. Vaughan, and F. M. O'Connor, Observation of near-zero ozone concentrations in the upper troposphere at midlatitudes, *Geophys. Res. Lett.*, *25*, 1173-1176, 1998.

Davis, D. D., et al., Assessment of ozone photochemistry in the western North Pacific as inferred from PEM-West A observations during the fall 1991, *J. Geophys. Res.*, *101*, 2111-2134, 1996.

De Pondeca, M. S. V., A. Barcilon, and X. Zou, The role of wave breaking, linear instability, and PV transports in model block onset, *J. Atmos. Sci.*, *55*, 2852-2873, 1998.

Dobson, G. M. B., Origin and distribution of the polyatomic molecules in the atmosphere, *Proc. R. Soc. London, Ser. A*, *236*, 187-193, 1956.

Douglass, A. R., et al., A three-dimensional simulation of the ozone annual cycle using winds from a data assimilation system, *J. Geophys. Res.*, *101*, 1463-1474, 1996.

Duan, J., and S. Wiggins, Fluid exchange across a meandering jet with quasiperiodic variability, *J. Phys. Oceanogr.*, *26*, 1176-1188, 1996.

Dyer, A. J., and B. B. Hicks, Global spread of volcanic dust from the Bali eruption of 1963, *Q. J. R. Meteorol. Soc.*, *94*, 545-554, 1968.

Eluskiewicz, J., et al., Residual circulations in the stratosphere and lower mesosphere as diagnosed from Microwave Limb Sounder data, *J. Atmos. Sci.*, *53*, 217-240, 1996.

Feely, H. W., and J. Spar, Tungsten-185 from nuclear bomb tests as a tracer for stratospheric meteorology, *Nature*, *188*, 1062-1064, 1960.

Hansen, G., et al., Evidence of substantial ozone depletion in winter 1995-1996 over Northern Norway, *Geophys. Res. Lett.*, *24*, 799-802, 1997.

Harvey, V. L., and M. H. Hitchman, A climatology of the Aleutian High, *J. Atmos. Sci.*, *53*, 2088-2101, 1996.

Harvey, V. L., M. H. Hitchman, R. B. Pierce, and T. D. Fairlie, Tropical high aerosol in the Aleutian anticyclone, *J. Geophys. Res.*, *104*, 6281-6290, 1999.

Hess, P., Mixing processes following the final stratospheric warming, *J. Atmos. Sci.*, *48*, 1626-1641, 1991.

Hess, P., and J. R. Holton, The origin of temporal variance in long-lived trace constituents in the summer stratosphere, *J. Atmos. Sci.*, *42*, 1455-1463, 1985.

Hibbard, W. L., and D. Santek, The VIS-5D system for easy interactive visualization, in *Proceedings of Visualization '90*, pp. 28-35, IEEE Comput. Soc. Press, Los Alamitos, Calif., 1989.

Hitchman, M. H., M. McKay, and C. R. Trepte, A climatology of stratospheric aerosol, *J. Geophys. Res.*, *99*, 20,689-20,700, 1994.

Hollingsworth, A., et al., Monitoring of observations and analysis quality by a data assimilation system, *Mon. Weather Rev.*, *114*, 861-879, 1986.

Holton, J. R., P. H. Haynes, M. E. McIntyre, A. R. Douglass, R. B. Rood, and L. Pfister, Stratosphere-troposphere exchange, *Rev. Geophys.*, *33*, 403-439, 1995.

Hoskins, B. J., M. E. McIntyre, and A. W. Robertson, On the use and significance of isentropic potential vorticity maps, *Q. J. R. Meteorol. Soc.*, *111*, 877-946, 1985.

Jascourt, S., Convective organizing and upscale development processes explored through idealized numerical experiments, Ph.D. dissertation, 267 pp., Univ. of Wis.-Madison, 1997.

Kida, H., A numerical investigation of the atmospheric general circulation and stratospheric-tropospheric mass exchange: II. Lagrangian motion of the atmosphere, *J. Meteorol. Soc. Jpn.*, *55*, 71-88, 1977.

Kiehl, J. T., and S. Solomon, On the radiative balance of the stratosphere, *J. Atmos. Sci.*, *43*, 1525-1534, 1986.

Langford, A. O., and S. J. Reid, Dissipation and mixing of small-scale stratospheric intrusion in the upper troposphere, *J. Geophys. Res.*, *103*, 31,265-31,276, 1998.

Lefevre, F., F. Figarol, K. Carslaw, and T. Peter, The 1997 Arctic ozone depletion quantified from three-dimensional model simulations, *Geophys. Res. Lett.*, *25*, 2425-2428, 1998.

Leovy, C. B., et al., Transport of ozone in the middle stratosphere: Evidence for planetary wave breaking, *J. Atmos. Sci.*, *42*, 230-244, 1985.

Manney, G. L., et al., Modeling ozone laminae in ground-based Arctic wintertime observations using trajectory calculations and satellite data, *J. Geophys. Res.*, *103*, 5797-5814, 1998.

Martin, J. E., Quasi-geostrophic forcing of ascent in the occluded sector of cyclones and the trowal airstream, *Weather Forecasting*, in press, 1999.

Mecikalski, J. R., and G. J. Tripoli, Inertial available kinetic energy and the dynamics of tropical plume formation, *Mon. Weather Rev.*, *126*, 2200-2216, 1997.

Minschwaner, K., et al., The bulk properties of isentropic mixing into the tropics in the lower stratosphere, *J. Geophys. Res.*, *101*, 1457-1461, 1996.

Mlynczak, M. G., C. J. Mertens, R. R. Garcia, and R. Portmann, A detailed evaluation of the stratospheric heat budget, 2. Global radiation balance and diabatic circulations, *J. Geophys. Res.*, *104*, 6039-6066, 1999.

Morgan, M. C., and J. W. Nielsen-Gammon, Using tropopause maps to diagnose midlatitude weather systems, *Mon. Weather Rev.*, *126*, 2555-2579, 1998.

Mote, P. W., T. J. Dunkerton, M. E. McIntyre, E. A. Ray, and P. H. Haynes, Vertical velocity, vertical diffusion, and dilution by midlatitude air in the tropical lower stratosphere, *J. Geophys. Res.*, in press, 1999.

Newell, R. E., J. W. Kidson, D. G. Vincent, and G. J. Boer, *The General Circulation of the Tropical Atmosphere and Interactions with Extratropical Latitudes, vol. 2*, 371 pp., MIT Press, Cambridge, Mass., 1974.

Ngan, K., and T. G. Shepherd, Chaotic mixing and transport in Rossby wave critical layers, *J. Fluid Mech.*, *334*, 315-351, 1997.

Orsolini, Y. J., et al., Layering in stratospheric profiles of long-lived trace species: Balloon-borne observations and modeling, *J. Geophys. Res.*, *103*, 5815-5826, 1998.

Palmen, E. and E. W. Newton, *Atmospheric Circulation Systems*, 603 pp., Academic, San Diego, Calif., 1961.

Pierce, R. B., T.D. Fairlie, E.E Remsberg, J.M. Russell III, and W.L. Grose, HALOE observations of the Arctic vortex during the 1997 spring: Horizonal structure in the lower stratosphere, *Geophys. Res. Lett.*, *24*, 2701-2704, 1997.

Pokrandt, P. J., G. J. Tripoli, and D. D. Houghton, Processes leading to the formation of mesoscale waves in the midwest cyclone of 15 December 1987, *Mon. Weather Rev.*, *124*, 2726-2752, 1996.

Postel, G. A., and M. H. Hitchman, Climatology of Rossby wave breaking along the subtropical tropopause. *J. Atmos. Sci.*, *55*, 359-373, 1999.

Proffitt, M. H., and R. J. McLaughlin, Fast-response dual-beam UV-absorption ozone photometer suitable for use on stratospheric balloons, *Rev. Sci. Instrum.*, *54*, 1719-1728, 1983.

Proffitt, M. H., J. J. Margitan, K. K. Kelly, M. Loewenstein, J. R. Podolske, and K. R. Chan, Ozone loss in the arctic polar vortex inferred from high-altitude aircraft measurements, *Nature*, *347*, 31-36, 1990.

Randel, W. J., Global atmospheric circulation statistics, 1000-1 mb, *NCAR Tech. Note 366*, 256 pp., Natl. Cent. for Atmos. Res., Boulder, Colo., 1992.

Rex, M., et al., In situ measurements of stratospheric ozone depletion rates in the Arctic winter 1991/1992: A Lagrangian approach, *J. Geophys. Res.*, *103*, 5843-5853, 1998.

Rosenfield, J. E., P. A. Newman, and M. R. Schoeberl, Computations of diabatic descent in the stratospheric polar vortex, *J. Geophys. Res.*, *99*, 16,677-16,690, 1994.

Schoeberl, M. R., et al., Reconstruction of the constituent distribution and trends in the Antarctic polar vortex from ER2 flight observations, *J. Geophys. Res.*, *94*, 16,815-16,845, 1989.

Shapiro, M. A., Turbulent mixing within tropopause folds as a mechanism for the exchange of chemical constituents between the stratosphere and the troposphere, *J. Atmos. Sci.*, *37*, 994-1004, 1980.

Thorncroft, C. D., B. J. Hoskins, and M. E. McIntyre, Two paradigms of baroclinic wave life cycle behavior, *Q. J. R. Meteorol. Soc.*, *119*, 17-55, 1993.

Trenberth, K. E., and J. G. Olson, An evaluation and intercomparison of global analyses from the National Meteorological Center and the European Centre for Medium-Range Weather Forecasts, *Bull. Am. Meteorol. Soc.*, *69*, 1047-1057, 1988.

Tripoli, G. J., An explicit three-dimensional nonhydrostatic numerical simulation of a tropical cyclone, *Meteorol. Atmos. Phys.*, *49*, 229-254, 1992a.

Tripoli, G. J., A nonhydrostatic numerical model designed to simulate scale interaction. *Mon. Weather Rev.*, *120*, 1342-1359, 1992b.

Volk, C. M., et al., Quantifying transport between the tropical and mid-latitude lower stratosphere, *Science*, *272*, 1763-1767, 1996.

Wallace, J. M., Trajectory slopes, countergradient heat fluxes and mixing by lower stratospheric waves, *J. Atmos. Sci.*, *35*, 554-558, 1978.

Warneck, P., *Chemistry of the Natural Atmosphere*, 757 pp., Academic, San Diego, Calif., 1988.

M. L. Buker, M. H. Hitchman, and G. J. Tripoli, Department of Atmospheric and Oceanic Sciences, University of Wisconsin-Madison, 1225 W. Dayton St., Madison, WI 53706. (e-mail: marcus@meteor.wisc.edu; matt@meteor.wisc.edu; tripoli@meteor.wisc.edu)

(Received January 27, 1999; revised June 28, 1999; accepted June 30, 1999.)